

COMPARATIVE ANALYSIS OF HEAT TRANSFER PERFORMANCE FOR VARIOUS FIN GEOMETRIES TO PERFORM THE OPTIMUM HEAT SINK

Z. S. Abdel-Rehim^{*} & Ashraf Lashine^{}**

^{*}Mechanical Engineering Department,
National Research Center,
El-Bohos St., Dokki, Giza, Egypt,
e-mail: zabdelrehim@yahoo.com

^{**}Mechanical Engineering Department,
Faculty of Engineering, Shoubra,
Banha University
e-mail: a.lashine@yahoo.com

ABSTRACT

The comparative analysis of the heat transfer performances for various commonly used fin geometries is investigated in this work. Design geometries are optimized for minimizing thermal resistance at moderate laminar air velocities. The basis of comparison was chosen to be a circular array of 1mm diameter pin-fins with a 2mm pitch. The pitch-to-width ratio of the other geometries was chosen to provide equal ratios of fin area to base area. Computational fluid Dynamic (CFD) simulation is carried out on a two-dimensional computational domain bounded by planes of symmetry parallel to the flow. The air velocity was in the range of 0.5 to 5m/s. A comparison of heat transfer coefficient and pressure drop is presented. The results showed that the staggered geometries perform better than inline. At lower values of pressure drop and pumping power, elliptical fins work best. At higher values of pressure drop and pumping power, circular pin-fins offer highest performance.

KEYWORDS: CFD code, correlation, forced convection, heat-sink, in-line and staggered arrangement, laminar flow and optimization of pin-fin geometry

1- INTRODUCTION

During many years, even decades, thermal management was seen as a final and secondary step of the design process of microelectronics components. With the increase in circuit density and power dissipation of integrated circuit chips and the microelectronic devices, electronic packages have underlined the need for employing effective cooling devices and

cooling methods to maintain the operating temperatures of electronics components at a safe and satisfactory level. Heat sinks are devices that enhance heat dissipation from a hot surface, usually the case of a heat-generating component, to a cooler ambient, usually air. For this reason, the comparison in geometry of pin-fin heat sinks is of interest and needs to be investigated to determine applicability as a general cooling product. The heat transfer of a finned heat sink is due to resistance of conduction, convection, and radiation. From the junction of the device, heat is transported by conduction from the device through the interface and into the heat sink from which heat is usually removed by means of convection and radiation cooling. A literature survey shows very few studies on the thermal performance of an elliptical pin-fin heat sink. Chapman et al. [1] made the comparison of thermal performance of different fin geometries. Cross-section pin-fin and straight or parallel plate fins were investigated and compared with elliptical pin-fin heat sink in their work. Fin efficiency and convective efficiency of different fin geometries, can be compared to help in selection of a heat sink. For a fair comparison of heat sink geometries, equal wetted area of the fins per unit base area will be used. The present work is meant to be a generalized comparison in which the effects of flow parameters (e.g. pressure drop) on the heat sink performance are investigated in terms of thermal resistance between the heat sink surfaces to the ambient air. The mechanisms that influence the heat transfer and pressure drop of various pin-fin heat sinks need to be understood. The numerical simulation procedure used in their work is described and results of various configurations are compared. Comparisons of round-elliptical-square-parallel fins appear seldom in the literature. Wirtz et al [2] were amongst the earliest ones to measure the performance of a pin-fin heat sink. In their work, experimental results were reported on the thermal performance of model fan-sink assemblies consisting of a small axial flow fan which impinges air on a square array of pin-fins. Cylinder, square, and diamond shape cross section pin-fins were considered. The overall heat sink thermal resistances, R , were evaluated at fixed applied pressure rise and fixed fan power. They concluded that cylindrical pin-fins give the best overall fan-sink performance. Elliptical pin-fin arrays were not studied in their investigation. In addition, only impinging flow drawn through the fin arrays was considered. Sparrow and Larson [3] performed experiments to determine per-fin heat transfer coefficients for a pin-fin array situated in an oncoming longitudinal

flow that turns to a cross-flow. They varied the geometric parameters of round fins including the fin height to diameter ratio (H/D) and the inter-fin pitch to diameter ratio (P/D). The pressure drop across the array was also measured and presented in dimensionless form relative to a specially defined velocity head, which gave a universal pressure drop result for all operating conditions. Subsequent to this study, they also compared the performance of different pin-fin geometries [4]. However, the objective was to determine which fin height and inter-fin spacing yield the lowest overall thermal resistance for the array. The minimization of the resistance was sought under the constraint of constant pumping power for all candidate systems (i.e. those characterized by different H/D and P/D values) and for a uniform fin-to-air-stream temperature difference for all fins in a given array. The optimal geometry of an array of fins that minimizes the thermal resistance between the substrate and the flow forced through the fins was reported by Bejan and Morega [5]. Both round pin-fin arrays and staggered parallel-plate fin arrays were optimized in two steps, first the optimal fin thickness was selected and then the optimal size of fluid channel was determined. They also compared the minimum thermal resistance of staggered parallel-plate arrays and continuous fins. Furthermore, the dimensionless pressure gradient was plotted against Reynolds number. Wirtz and Colban [6] simulated electronic packages to compare the cooling performance of inline and staggered parallel-plate arrays for both sparse and dense packaging configurations. They found that staggered arrays exhibit higher element heat transfer coefficients and friction factors than inline arrays at a given flow rate. However, no significant difference in performance was observed between staggered and in-line configurations when they were compared based on either equal coolant flow pressure drop or pumping power. They did not change the element or channel geometry and therefore the effect of these parameters on their results is not known. Inline and staggered parallel-plate arrays were also investigated, both numerically and experimentally, by Sathyamurthy et al [7]. They obtained a good agreement between their numerical results and experiments. Their results illustrated that the thermal performance of the staggered fin configuration was better than the planar fin configuration over the power and flow ranges examined. This enhanced thermal performance, however, was realized at the expense of an additional pressure drop. Heat transfer enhancement mechanisms in inline and staggered parallel plate fin heat exchangers

were also studied by Zhang et al [8] who examined the geometry effects. There are also a few reports on the thermal performance and the flow bypass effects of parallel plate fin arrays. Barrett and Obinelo [9] studied tip clearance and span-wise spacing across a range of approach flow rates and fin densities. Wirtz et al [10] also studied the effect of flow bypass on the performance of longitudinal fin heat sinks. Iwasaki et al [11] studied the cooling performance of this typical heat sink by using numerical, experimental and nodal network techniques. Keyes [12] studied forced convection through parallel plate fins, while natural convection in the same geometry was studied by Culham et al [13]. Design of an optimal pin fin heat sink with air impingement cooling [14]. The velocity range considered only covers laminar flow conditions. An extension to turbulent flow will be considered in the future. A critical review of extended surface heat transfer [15]. Heat Transfer Enhancement by Pin Elements is performed by Sahiti et al. [16].

In this work, a comparative analysis of the heat transfer performance of circular, square, elliptical pin-fin and parallel plate heat sinks and compare the results on a meaningful and fair basis are investigated. Both in-line and staggered arrays of different geometry fins are considered. In total, seven different two-dimensional geometries i.e., in-line cylindrical, staggered cylindrical, in-line square, staggered square, parallel plate, staggered parallel plate, and staggered elliptical are modeled. Numerical simulations are performed using Computational Fluid Dynamics (CFD) code [17] and [18]. The code uses the finite volume method approach and employs the SIMPLEC velocity-pressure coupling algorithm.

4- PARAMETERS AND GEOMETRY

As noted above, we have considered seven different geometries. In order to make a fair comparison for the purpose of optimizing heat transfer rate some parameters are fixed for all geometries. These parameters are: the fin cross-sectional area per unit base area, the wetted surface area per unit base area, and the flow passage area. However, for the sake of generalizing a fair and meaningful approach, the parameters in this case are all based on a per unit base area.

The surface temperature of the pin is $T_w (>T_a)$ in the case of the isothermal fin and the heat flux is Q for the isoflux boundary condition. Following restrictions are imposed on the analysis:

$$\begin{aligned} Pr &\geq 0.71 \\ 40 &\leq Re \leq 1000 \end{aligned}$$

$$\begin{aligned} 1 &\leq U_{app} \text{ (m/s)} \leq 6 \\ 1 &\leq D(\text{mm}) \leq 3 \end{aligned}$$

$$1.25 \leq S_L \leq 3$$

The commonly used in-line circular array of fins with 1mm pin diameter (w) and a 2mm pitch and span-wise and length-wise as ($P_S=P_L$) has been selected to be the base case for comparison, Fig. (1) This yields a fin cross-sectional area per base area as shown below.

$$A_{section} = \frac{\pi w^2 / 4}{P_S \times P_L} = \frac{4}{\pi} \left(\frac{w}{P_S \times P_L} \right)^2 \quad (1)$$

So, the flow passage area (A_{flow}) per unit base area becomes:

$$A_{flow} = 1 - A_{section} \quad (2)$$

And the wetted perimeter (P_{wet}) per unit base area of fin is:

$$P_{wet} = \frac{\pi w}{P_S \times P_L} \quad (3)$$

These three values are chosen to be fixed for all geometries considered here. The hydraulic diameter (D_h) is determined from the flow passage area:

$$D_h = 4 \left(\frac{A_{flow}}{P_{wet}} \right) \quad (4)$$

For the case of parallel plates, this is equal to twice the plate spacing. This differs from the traditional use of tube diameter for circular tube arrays, but is necessary to reflect the nature of internal flow and permit comparison of a variety of fin geometries. The Reynolds number (Re) is based on the hydraulic diameter and the heat sink approach velocity, $V_{approach}$.

$$Re = \frac{\rho \times v_{approach} \times D_h}{\mu} \quad (5) \quad Nu = \frac{h D_h}{k} \quad (6)$$

Friction coefficient, C_f , is calculated as a function of pressure gradient in heat sink using heat sink approach velocity as reference, Equation (7).

$$C_f = \frac{\left(\frac{\Delta P}{L} \right) D_h}{4 \left(\frac{1}{2} \rho v_{approach}^2 \right)} = \frac{\left(\frac{\Delta P}{L} \right) D_h}{2 \rho v_{approach}^2} \quad (7)$$

5- CFD MODELING

The governing equations are those of two-dimensional continuity, Navier-Stokes and the energy equation in their incompressible laminar form. These equations are well known and

will not be repeated here. The details and solution method are given in [14]. Since an array of fins is considered, the most suitable boundary condition for the inlet and outlet of the computational domain is a periodic one. In the transverse direction, symmetry condition is used. For the thermal boundary condition on the solid surfaces, an isothermal condition is imposed. All fluid (i.e. air) properties are assumed to be constant. The CFD code was used for the simulation. The computational mesh was generated using triangular elements. In order to accurately resolve the solution fields in the high gradient regions, the grid was stretched. In addition to stretching, adaptive solution algorithms were used to ensure an accurate resolution of the temperature and velocity gradients. The discretization scheme was second order accurate. A SIMPLEC velocity-pressure coupling multi-grid solution procedure was used. For the simulations presented here, depending on the geometry used, fine meshes of up to 40,000 elements were used. Set of parameters and data of the CFD code numerical model are mentioned as the following:

- Solver: Segregated Formulation: Implicit Time: Steady state, Flow model: Laminar
- Radiation model: No
- Operating temperature: 300 K
- Gravitational acceleration: $y = -9.81 \text{ m/s}^2$,
- Walls: smooth walls
- Solutions controls: (Discretization methods)
- Pressure – velocity coupling: Simple Energy: First order upwind

6- POWER DISSIPATION AND TEMPERATURE DIFFERENCE IN NATURAL CONVECTION:

A clear correlation between the power dissipation and the temperature difference in heat transfer by natural convection is widely accepted [19] and [20]. The next Equations show the nature of this correlation, see Equations (5-9). The expressions (5) and (6) represent the dimensionless local heat transfer coefficient (Nusselt Number) for natural convection in a vertical plate. Where h is the local convection heat transfer coefficient, x is the reference length (height), k is the thermal conductivity of the fluid, Pr is Prandtl Number, and Gr_x is the Local Grashof Number (see Equation (7)).

$$Nu_x = 0.5 Pr^{\frac{1}{2}} (0.95 + Pr)^{-\frac{1}{4}} \times Gr^{\frac{1}{4}} \quad (5)$$

$$h_x = \frac{Nu_x k}{x} \quad (6)$$

$$Gr_x = \frac{g \beta (T_w - T_\infty) x^3}{\nu^2} \quad (7)$$

Where g is the acceleration of gravity, β is the thermal expansion coefficient of the fluid, T_w is the surface (wall) temperature, T_∞ is the fluid free-stream temperature, and ν is the kinematic viscosity of the fluid. The Prandtl Number expresses the ratio of fluid velocity boundary layer thickness to the fluid temperature boundary layer thickness, and the Grashof Number the ratio of fluid buoyancy stress to viscous stress. The following expression is obtained from Newton's Law of Cooling:

$$h = \frac{Q}{A (T_w - T_\infty)} = \frac{1}{L} \int_0^L h_x dx = \frac{4}{3} \left(\frac{Nu_L k}{L} \right) = \frac{4}{3} h_{x=L} \quad (8)$$

Substituting the expressions (7), and (8) in the equation (6) one obtains the equation (9), which shows that the power dissipation is proportional to the 5/4 power of the temperature difference.

$$Q = 0.68 Pr^{\frac{1}{2}} \frac{A k}{L} (0.95 + Pr)^{-\frac{1}{4}} \frac{(g \beta)^{\frac{1}{4}} L^{\frac{3}{4}} (T_w - T_\infty)^{\frac{5}{4}}}{\nu^{\frac{1}{2}}} \quad (9)$$

The equation (9) constitutes the basic expression to calculate the power dissipated for a vertical plate by natural convection.

7-RESULTS AND DISCUSSIONS

The geometry results were obtained at various air velocities in the range of 0.5 to 5 m/s. Since the hydraulic diameter was fixed as noted previously, this covered a fixed range of Reynolds number for the selected geometry. The horizontal boundaries of the computational domain are symmetry boundary conditions. The computational module is assumed to be well within the bank of fins and hence the inlet and outlet boundaries are

considered to be of a periodic type. Reynolds number by refining it as well as using local solution adaptation features of the code. A sample of computed contours of the axial velocity and temperature distribution for the base case (inline circular fin) at $Re = 260$ is shown in Figs. (2) and (3). Figures (4-6) show the obtained temperature distribution in different parts of the model as well as the velocity vectors in the plane $x - y$ adjacent to the plate. It is clear, that the temperature distribution in the plate is not homogeneous and hence one should expect that the power dissipation is no longer proportional to the $5/4$ (1.25) power of the temperature difference. This temperature difference is obtained using the maximum temperature of the plate. This is logic since, in microelectronics thermal management; the maximum temperature of the component is always the parameter to be controlled. To find out if the previous assumption is true, look to the graphic representation in the Fig. (7). It is noticed that the power dissipation is proportional to the 1.08 power of the temperature difference. This result supports the correlation, power density $\approx (T_w - T_o)^{1.25}$, where T_o and T_w are operating and wall temperatures, this correlation is widely accepted in all the literature about natural convection, and will not be valid any longer for non - isothermal surfaces. Therefore, together with the values obtained from the simulations, two lines have also been plotted, representing the correlations: Power density $\approx \Delta T^{1.25}$ and Power density $\approx \Delta T^{1.00}$. In this way the divergence between the theory and the simulated results is more evident. As a final conclusion, one can say that the relation between power density and temperature difference (ΔT) fit better with a linear relation than with $\Delta T^{5/4}$ (Equation (9)). A comparison of the average Nusselt number variation with Reynolds number for various geometries is shown in Figs. (8) and (9). For clarity, the results are not plotted on a single graph and are grouped into two. The in-line and staggered geometries are compared in Fig. (8), and the various staggered shapes are compared in Fig. (9). Seven simulations were carried out for the selected geometry by varying the air-flow rate. The curves represent the lines of best fit through the seven points obtained in the simulations. It can be noted that the staggered circular fin shape yields the highest Nusselt number at all Reynolds numbers in the range considered here. The lowest Nusselt number is for that of parallel plate and staggered plate arrangements, with the former showing a milder Reynolds number dependence than the latter. Figure (8) shows obviously that the parallel plate configuration lead to a Nusselt number which is much

lower than the other configurations. It is interesting to note that the staggered elliptic fins are only marginally better than the staggered plate. In order to compare the fan power requirements of the selected geometry, the friction is plotted in Fig. (10). Relative differences are nearly constant for all geometries throughout the range of velocities studied except for the parallel plate. The parallel plate exhibits the lowest pressure drop, whereas the staggered circular is the worst configuration (note that this has the highest heat transfer coefficient). The heat transfer coefficient versus pressure gradient is shown in Fig. (11). It is noted that the results are presented in this figure in dimensional form. The seven points on each line of best fit correspond to the seven Reynolds numbers simulated (i.e. $Re=110, 175, 260, 390, 590, 880, \text{ and } 1320$). The different geometries can then be compared in terms of thermal performance as a function of pressure drop. At a given pressure drop, the staggered plate and staggered elliptic heat-sinks permit more air-flow. At lower flow rates, these geometries provide higher heat transfer. At higher values of pressure gradient, above 0.01 Pa/m , the staggered circular and square geometries show the highest performance. Throughout the range of flow rates studied, the inline geometries performed poorly. In all cases, circular pin fins out-perform square pin fins and elliptical fins out-perform plate fins. Throughout the range of velocities, staggered plate fins show higher pressure drop and lower heat transfer than staggered elliptic fins. Square pins have pressure drop comparable to that of circular pins but lower heat transfer. Figure (12) shows heat transfer plotted against pumping power. Since pumping power is the product of volume flow rate and pressure drop, this is a third constraint on flow (constant volume flow rate and pressure drop have already been considered). This results in shifts in the relative performance of the various geometries. The staggered plate configuration offers the highest conductance at fixed pumping power throughout the range of flow rates studied, while parallel plate fins offers the lowest. In general, the geometries providing the highest heat transfer coefficients do so at the expense of excessive pressure drop.

8- CONCLUSIONS

The comparison of various heat-sink geometries has been presented. In general, it is found that rounded geometries out-perform similar sharp-edged fin shapes. In all cases, staggered geometries perform better than inline. At lower values of pressure drop and pumping

power, elliptical fins work best. At higher values of pressure drop and pumping power, circular pin-fins offer highest performance.

In this study, the ratio of fin cross-sectional area to base area was kept constant at just below 20%. Additionally, the lengthwise fin pitch was held equal to the span-wise pitch. Both of these constraints can be relaxed in future studies, increasing the number of parameters available and greatly increasing the complexity of the problem. Another issue is that of the periodic boundary condition. This provides a conservative lower bound on both heat transfer and pressure drop. The degrees to which these are under-predicted depend on the fin geometries and the length of the heat-sink relative to the entry region. The relation between power density and temperature difference (ΔT) fit better with a linear relation than with $\Delta T^{5/4}$

Nomenclature

A_{flow}	Area of air flow passage per base area
$A_{\text{sectional}}$	Fin cross-sectional area per base area
C_f	Friction coefficient
D_h	Hydraulic diameter (mm)
h	Surface heat transfer coefficient (W/m ² K)
k	Thermal conductivity of air (W/m K)
Nu	Nusselt number
P_{drop}	Pressure drop (Pa)
P_L	Length-wise pitch (mm)
P_S	Span-wise pitch (mm)
Pr	Prandtl number
$(\Delta P/L)$	Pressure drop per unit length (Pa/m)
P_{wet}	Fin perimeter per base area (mm ⁻¹)
Re	Reynolds number
T_o and T_w	Operating and wall temperatures
ΔT	Temperature difference
v_{approach}	Heat sink approach velocity (m/s)
w	Fin width (mm)

Greek symbol

ρ	Density of air (kg/m ³)
μ	Dynamic viscosity of air (kg/m s)
ν	Kinematic viscosity of the fluid

REFERENCES

1. Chapman C. L., S. Lee, and B. L. Schmidt, "Thermal Performance of an Elliptical Pin Fin Heat Sink," Proceedings of the Tenth IEEE Semi-Thermo Symposium, pp. 24-31, 1994
2. Wirtz R. A., R. Sohal, and H. Wang, "Thermal Performance of Pin-Fin Fan-Sink Assemblies," Journal of Electronic Packaging, Vol. 119 pp. 26-31, 1997
3. Sparrow E. M. and E. D. Larson, "Heat Transfer from Pin-Fins Situated in an Oncoming Longitudinal Flow which Turns to Cross-flow," International Journal of Heat and Mass Transfer, Vol. 25, No. 5, pp. 603-614, 1982
4. E. D. Larson and E. M. Sparrow, "Shorter Communications in Heat Transfer from Pin-Fins Situated in an Oncoming Longitudinal Flow which Turns to Cross-flow," International Journal of Heat Mass Transfer, Vol. 25, No. 5, pp. 723-725, 1982
5. A. Bejan and A. M. Morega, "Optimal Arrays of Pin Fins and Plate Fins in Laminar Forced Convection," Journal of Heat Transfer, Vol. 115, pp. 75-81, 1993
6. Wirtz R. A. and D. M. Colban, "Comparison of the Cooling Performance of Staggered and In-Line Arrays of Electronic Packages," Journal of Electronic Packaging, Vol. 118, pp. 27-30, 1996
7. Sathyamurthy P., P.W. Runstadler, and S. Lee, "Numerical and Experimental Evaluation of Planar and Staggered Heat Sinks," Proceedings of the Fifth Inter-Society Conference on Thermal Phenomena in Electronic Packaging, pp. 132-139, 1996
8. Zhang L. W. "Heat Transfer Enhancement Mechanisms in Inline and Staggered Parallel-Plate Fin Heat Exchanger," International Journal of Heat and Mass Transfer, Vol. 40, No. 10, pp. 2307-2325, 1997
9. Barrett A. V. and I. F. Obinelo, "Characterization of Longitudinal Fin Heat Sink Thermal Performance and Flow Bypass Effects Through CFD Methods," Proceedings of the Thirteenth IEEE Semi-Therm Symposium, pp. 158-164, 1997
10. Wirtz R. A, W. Chen, and R. Zhou, "Effect of Flow Bypass on the Performance of Longitudinal Fin Heat Sinks," Journal of Electronic Packaging, Vol. 116, pp. 206-211, 1994
11. Iwasaki H., T. Sasaki, and M. Ishizuka, "Cooling Performance of Plate Fins for Multi-chip Modules," IEEE Transaction on Components, Packaging, and Manufacturing Technology - Part A, Vol. 18, No. 3, pp. 592-595, 1995
12. Keyes R.W., "Heat Transfer in Forced Convection Through Fins", IEEE Transactions on Electron Devices, Vol. 31, No. 9, pp. 1218-1221, 1984
13. Culham J. R., M. M. Yovanovich, and S. Lee, "Thermal Modeling of Isothermal Cuboids and Rectangular Heat Sinks Cooled by Natural Convection", IEEE Transactions on Components, Packaging, and Manufacturing Technology -Part A, Vol. 18, No. 3, pp. 559-566, 1995
14. Maveety, J.G., Jung, H. H., "Design of an optimal pin fin heat sink with air impingement cooling", Heat & Mass Transfer Vol.27 No.2, pp. 229-240, 2000
15. Razelos, P., "A Critical Review of Extended Surface Heat Transfer", Heat Transfer Engineering, 24(6): pp. 11-28, 2003.
16. Sahiti, N. Durst, F. and Dewan, "A. Heat Transfer Enhancement by Pin Elements", Int. J. Heat Mass Transfer, pp. 4738-4747, 2005.
17. FLUENT/UNS User's Guide, Fluent Incorporated, Lebanon, New Hampshire, 1996
18. Wesseling P., "Principles of Computational Fluid Dynamics", Springer-Verlag, Berlin, pp 1-261, 2001
19. Holman J. P, "Heat Transfer", McGraw-Hill Companies INC, New York, pp 150-258, 1998
20. Culham J. R "Natural Convection Modeling of Heat Sinks Using Web-Based Tools", Journal of Electronics Cooling, Vol. 6, no 3, pp 44-51, 2000

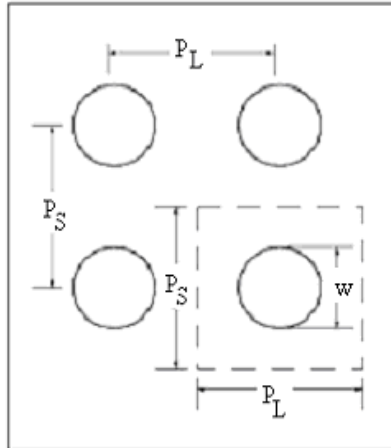


Fig. (1): Parameters of in-line circular pin fin.

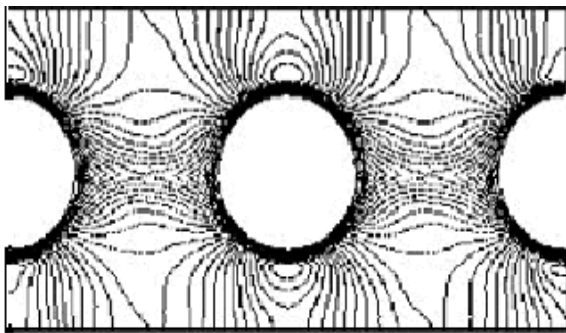


Fig. (2): Contours of u-velocity of in-line circular pin-fin at $Re = 260$.

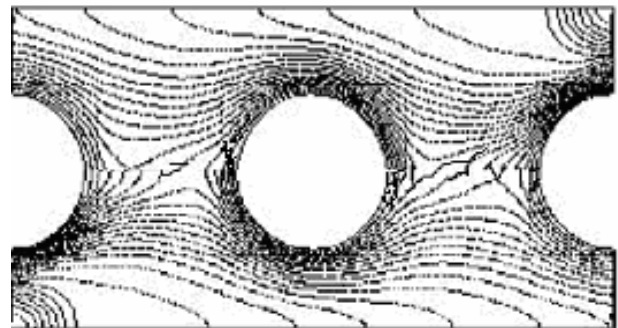


Fig. (3): Contours of temperature of in-line circular pin-fin at $Re = 260$.

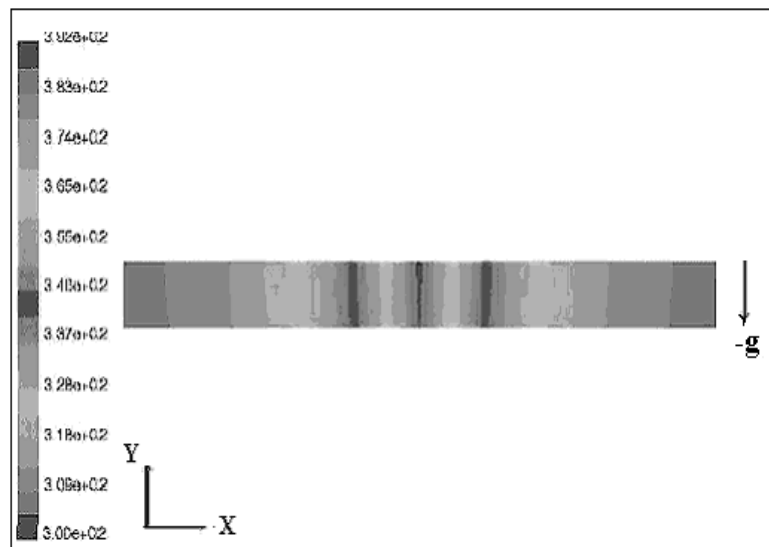


Fig. (4): Static temperature distribution in the plate for power dissipation, 2.5 watts.

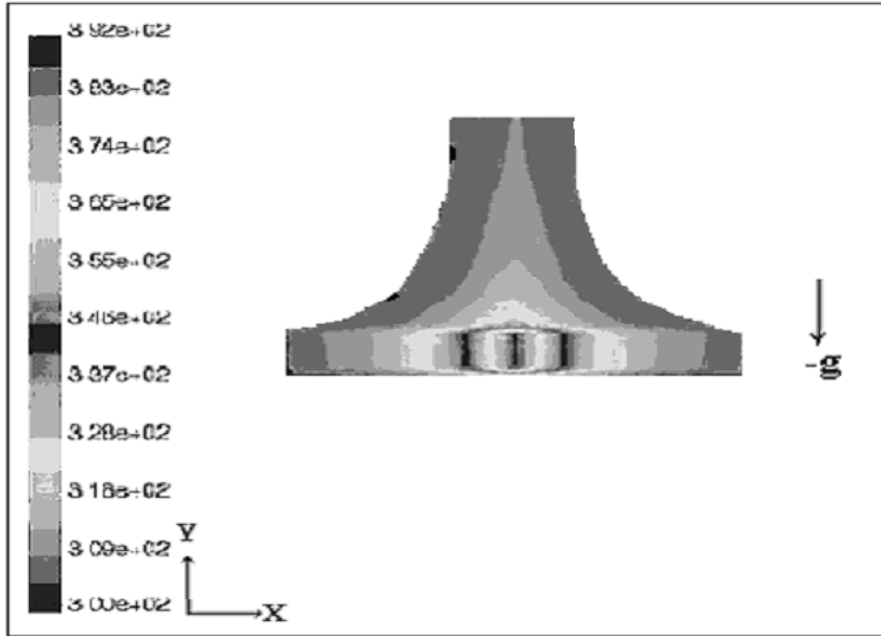


Fig. (5): Static temperature distributions for the plane $x - y$, adjacent to the plate using power dissipation, 2.5 watts

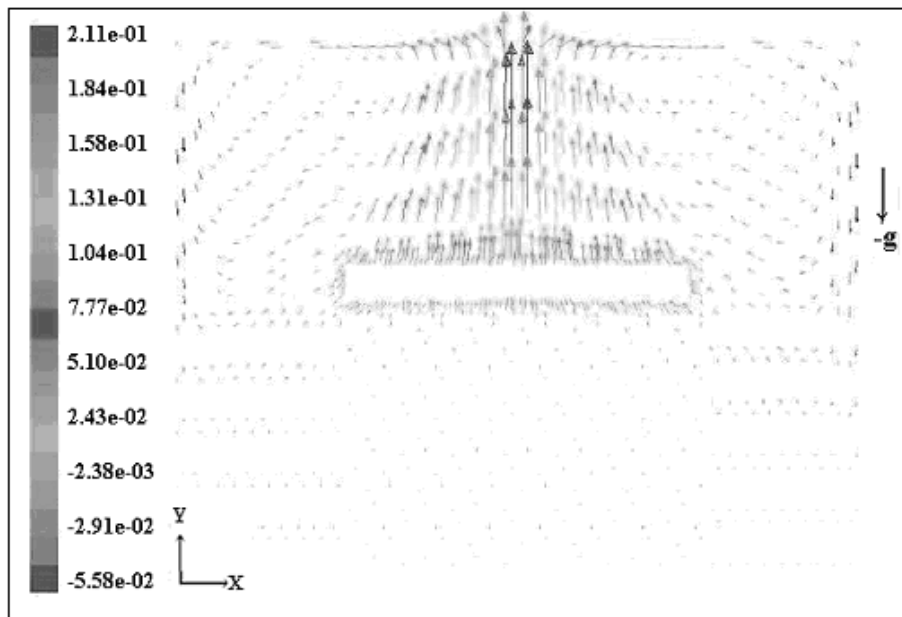


Fig. (6): Velocity vectors colored by x-velocity for plane $x - y$, adjacent to the plate using power dissipation, 2.5 watts.

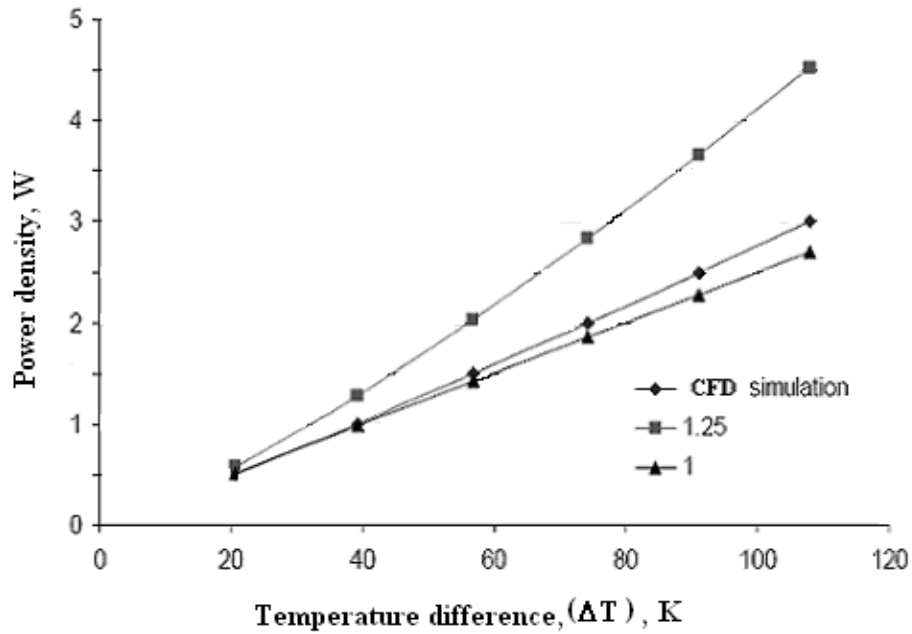


Fig. (7): Variation of power densities and their corresponding temperature difference in the plate.

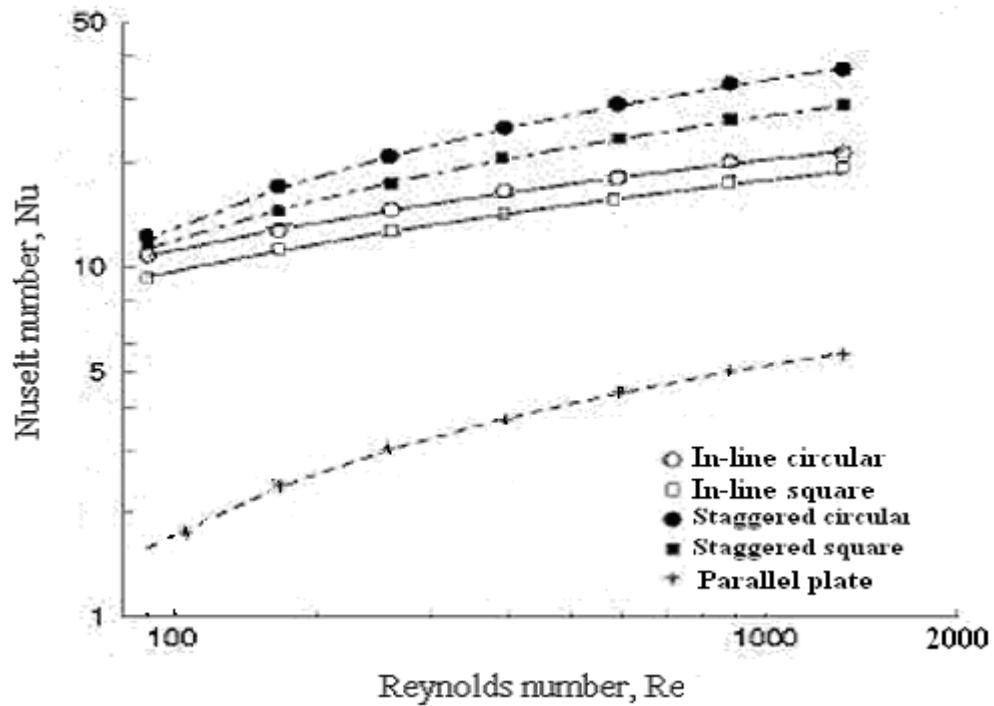


Fig. (8): Nusselt number vs. Reynolds number for in-line and staggered geometries of circular and square fins and the parallel plate.

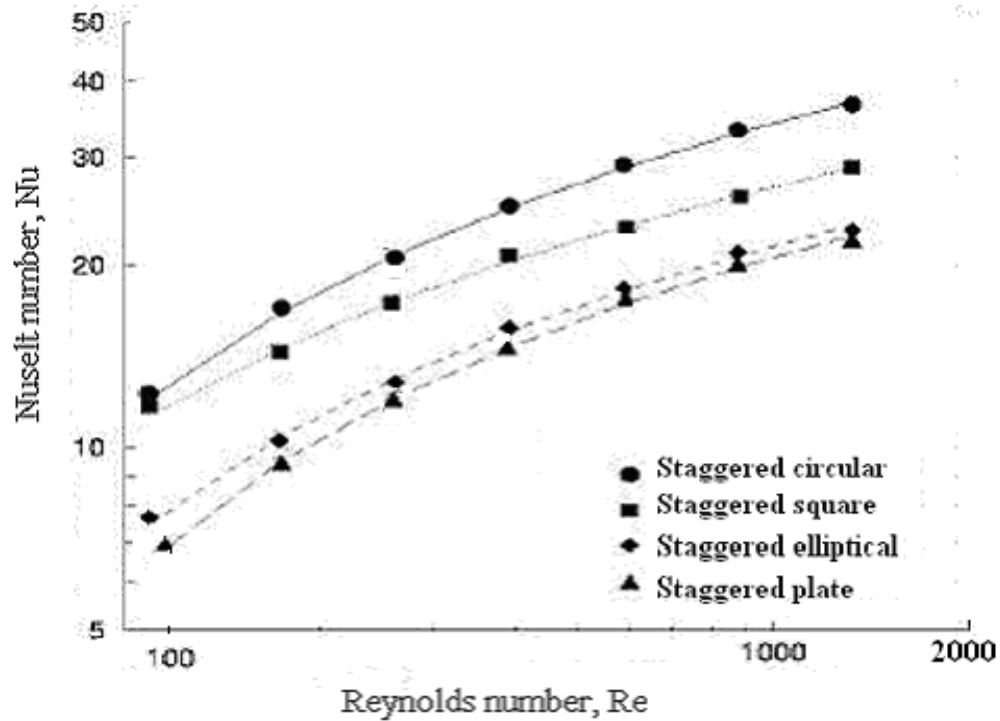


Fig. (9): Nusselt number vs. Reynolds number for staggered fins.

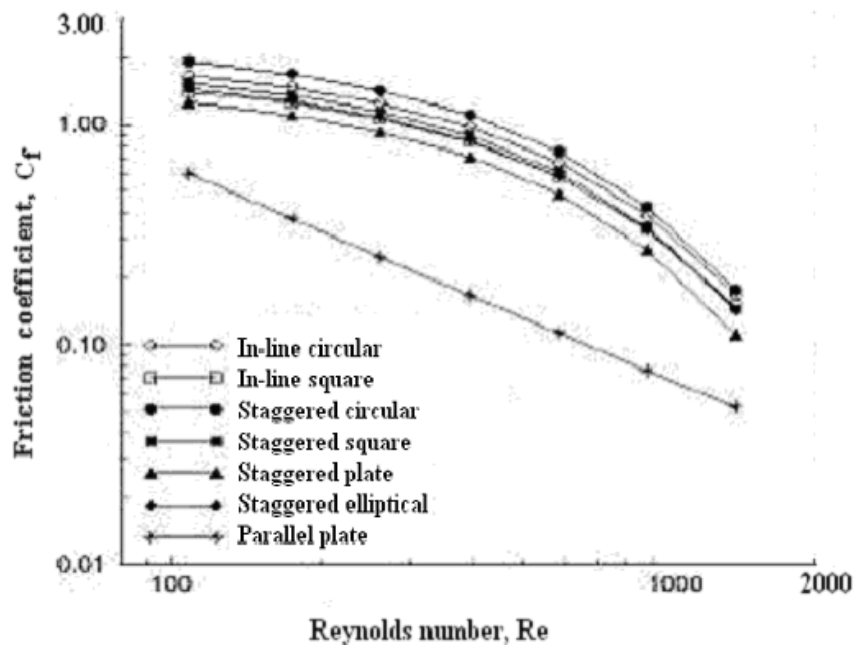


Fig. (10): Friction coefficient vs. Reynolds number for the selected fin geometries.

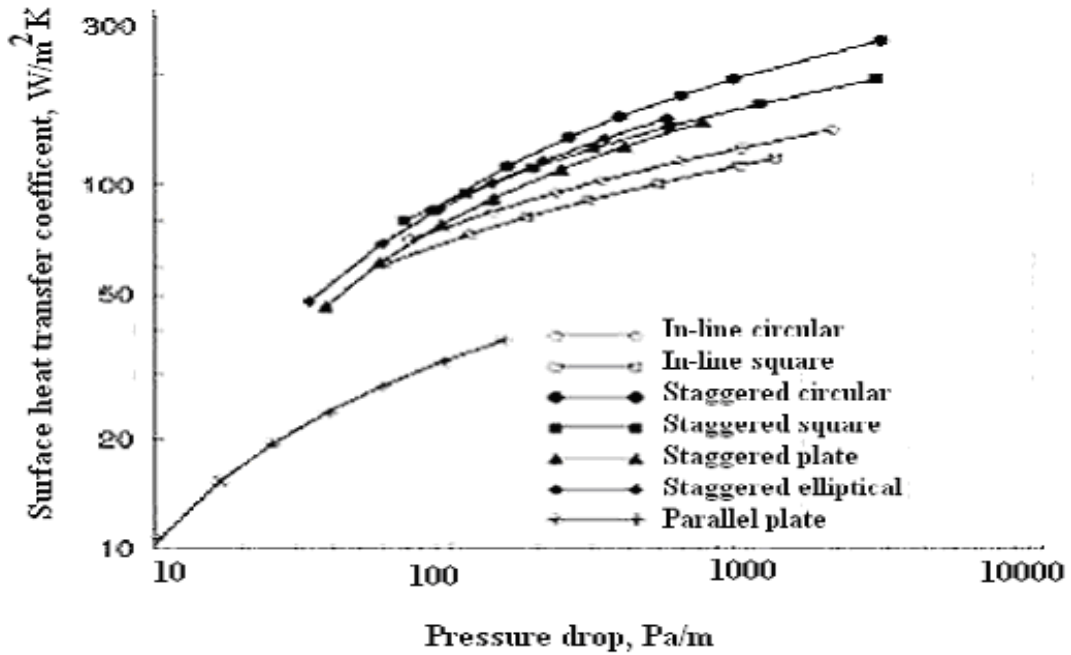


Fig. (11): Variation of surface heat transfer coefficient vs. pressure drop for the selected fin geometries.

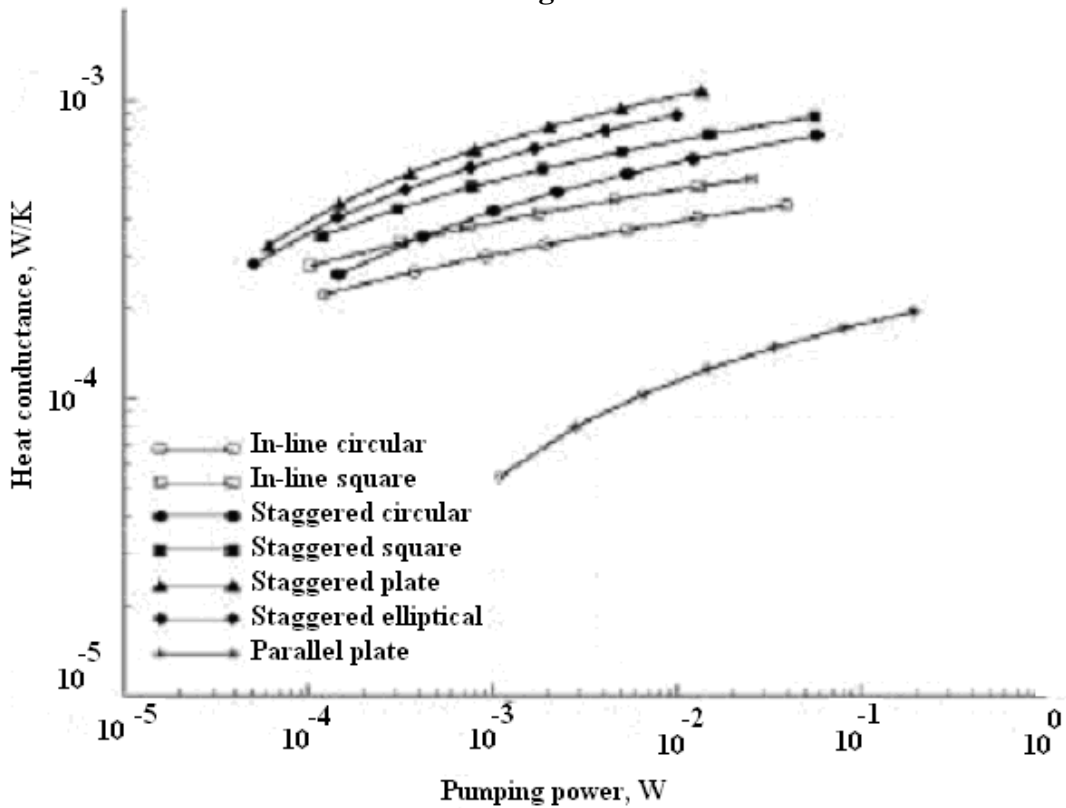


Fig. (12): Variation of heat conductance vs. pumping power for the selected fin geometries.